Experimental Investigation of the Flow Behavior of Ionic Liquids for use as Working Fluids in Enhanced Geothermal Systems

Christian Akhilome, Sushobhan Pradhan, and Prem Kumar Bikkina

Oklahoma State University

Keywords: *Enhanced geothermal systems, Ionic liquids, microfluidics, thermal short-circuiting*

Abstract

The heat recovery efficiency of an enhanced geothermal system (EGS) relies on the flow dynamics of the circulated working fluid in the natural and engineered fractures within the reservoir. The use of Ionic liquids (ILs) as geothermal working fluids is a promising alternative to conventional working fluids such as water due to their favorable properties including wide liquid range, high thermal stability, and shear thinning behavior. ILs are expected to offer enhanced flow hydraulics and address thermal short-circuiting, a potential issue in EGS operations. ILs dynamically adjust their rheological properties in response to localized temperature changes, enabling them to selectively traverse higher temperature flow paths with minimal resistance. Consequently, ILs can potentially eliminate flow shortcuts, thereby improving the overall heat recovery from the EGS.

This study investigates the flow behavior of ILs and their performance in EGS. Specifically, it examines correlations between flowrates and pressure drops of two ILs, viz., 1-butyl-3-methyl-imidazolium bromide ([bmim][Br]), and 1-hexylpyridinium bromide ([hPy][Br]), within idealized micro fractures. Experimental evaluations were conducted using a microfluidic set-up to simulate flow through micro channels in EGS, utilizing a variety of fluid samples, including De-ionized (DI) water, and 5%, 10%, and 25% solutions of [bmim][Br] and [hPy][Br]. Furthermore, the study also investigated the high-temperature flow behavior of [bmim][Br] at 18 ºC, 50 ºC, and 80 ºC, comparing it to the performance of DI water under the same conditions. The reduction in the frictional pressure drops of the IL is compared to that of DI water, revealing significant hydrodynamic improvements with the IL. Particularly, as temperature increased, the IL showed better performance over DI water in terms of reduction in frictional pressure loss within the microchannels with an average reduction approximating four times larger than that of DI water. This research enhances our understanding of IL flow behavior in microchannels, which is crucial for optimizing heat recovery from EGS and advancing sustainable and cost-effective geothermal operations.

1. Introduction

The vast thermal energy resources found in the Earth's subsurface offer considerable potential for green and sustainable power generation. This thermal energy is mainly generated from heat conduction and convection from the Earth's core and exothermic decay of radioactive elements (Emujakporue, 2017). Bertani (2016) estimates that harnessing 1% of the Earth's crust heat could power the world for about three millennia, underscoring its enormity. Furthermore, the replenishment rate exceeds depletion, emphasizing the sustainability of geothermal energy. However, most high geothermal gradient areas are located within igneous rocks with very low permeabilities which makes harnessing this energy very challenging. Thus, the concept of enhanced geothermal systems (EGS) was developed to exploit these vast resources by creating flow paths that permit heat extraction from these reservoirs. EGS involves artificially stimulating hot dry rock (HDR) reservoirs to create a subsurface fracture network that allows circulation of a working fluid, traditionally water, between an injection well and a production well. Heat is exchanged from the HDR to the working fluid which is produced to the surface through the production well. Depending on the temperature of the produced fluids, they can be used for different purposes such as space heating for geothermal fluid temperatures as low as 80 ^{o}C and about 180 ^{o}C for economical electricity generation (Smith et al., 1975).

The efficiency of EGS is dependent on the temperature of the extracted fluid. Higher temperatures indicate better performance (Asai et al., 2019). The properties of the circulated working fluid are crucial for optimizing heat recovery from geothermal reservoirs. Various working fluids have been explored to improve the performance of EGS, with water and CO_2 being the most commonly used. Although water is relatively cheaper than other working fluids, its use in EGS is limited by issues related to mineral dissolution and precipitation. However, water does have higher thermal conductivity and specific heat capacity compared to CO_2 (André et al., 2006; Brown, 2000). Supercritical CO_2 ($ScCO_2$ – occurs when CO_2 is held above its critical temperature and pressure), prevents the silica precipitation and mineral dissolution challenges associated with water-based EGS projects. Furthermore, $ScCO_2$ yields a higher mass flow rate and net heat extraction for a given injection rate in EGS due to the existence of thermal siphoning between injection and production wells (T. Guo et al., 2019; Lei, 2022; Olasolo et al., 2016; Sun et al., 2018). In addition, unlike water, fluid losses in geothermal reservoirs may be beneficial when CO_2 is used as the working fluid due to the possibility of carbon sequestration, depending on suitable site conditions. A prevalent issue with both CO_2 and water geothermal working fluids is the possibility of flow channeling which can lead to early thermal breakthrough. Formation heterogeneities often lead to the creation of fractures with non-uniform properties when geothermal reservoirs are stimulated. This often leads to the creation of preferential flow paths in EGS due to the uneven hydraulic conductivities of the induced fractures (Gischig & Preisig, 2015; T. Li et al., 2016). Since preferential flow paths allow more flow compared to other fractures, the temperature of the surrounding rock decreases more rapidly. This cooling causes an increase in the fracture aperture due to thermal destressing, which in turn leads to even more channelized flow (Fu et al., 2016; B. Guo et al., 2016). This phenomenon, called thermal short-circuiting, can result in insufficient heat exchange and early thermal breakthroughs, leaving a large volume of reservoir rock untouched (S. Li et al., 2022). As a result, the temperature of the produced fluids reduces, thereby compromising the economic viability of the EGS project. Numerous field studies have documented evidence of thermal short-circuiting in EGS. For instance, Lu (2018) reviewed prominent EGS sites worldwide and noted that thermal short-circuiting contributed to the inability of projects like Rosemanowes

in the UK and Hijiori in Japan to achieve their target heat production over time, ultimately leading to the termination of operations at both sites. Different approaches have been suggested to mitigate thermal short-circuiting in literature including the use of temperature-sensitive proppants to modify fracture conductivity (Al Balushi et al., 2023; Hu et al., 2021), periodic shut-ins of injectors and producers (Fan et al., 2020), and the use of chemicals to plug highly conductive fractures (Zhang & Dahi Taleghani, 2023). However, there has been insufficient evidence to support the applicability of these remedies in practical terms.

Recently, ionic liquids (ILs) have been garnering significant attention in various fields, including thermal energy storage and EGS. ILs are salts composed entirely of ions and are generally liquids below 100 ^{o}C. ILs have emerged as promising alternatives to water and CO_2 due to their unique properties such as high thermal and chemical stability, low melting point, low vapor pressure, and shearing thinning which are favorable for EGS applications. Unlike water and $ScCO_2$, ILs significantly vary their rheological properties in response to temperature changes in the fractures which can potentially eliminate flow shortcuts. The underlying concept is that the viscosity of the ILs increases significantly when the temperature of the bounding rock matrix in channelized flow paths reduces. This increases the hydraulic resistance to flow in the preferential flow paths which leads to a redistribution of the working fluid into other regions in the EGS, thus, eliminating thermal shortcuts (Atashnezhad et al., 2023; Momoh et al., 2023). Despite this enormous potential, there is a relative scarcity of studies investigating the use of ILs as geothermal working fluids.

In this study, we investigated the performance of two ILs: 1-butyl-3-methyl-imidazolium bromide ([bmim][Br]) and 1-hexylpyridinium bromide ([hPy][Br]) as potential working fluids for EGS applications. We conducted a series of flowrate vs. pressure drop experiments using a microfluidic setup to mimic flow through a geothermal reservoir. Various fluid samples, including deionized (DI) water, and 5%, 10%, and 25% solutions of [bmim][Br] and [hPy][Br], were tested. Additionally, the study explored the high-temperature flow behaviors of [bmim][Br] at 18 °C, 50 °C, and 80 °C, comparing them to the performance of DI water under the same conditions. Our findings enhance the understanding of the flow behavior of ILs in microchannels, which is crucial for optimizing heat recovery from EGS and advancing sustainable and cost-effective geothermal operations. This research aims to contribute to the optimization of EGS by providing valuable insights into the flow dynamics of ILs as working fluids, potentially leading to more efficient and sustainable geothermal energy extraction methods.

2. Materials And Methods

2.1 Microchip

In this work, a 45 x 15 mm borosilicate glass microchip with three flow channels of varying widths was utilized. The microchip was designed and fabricated by Micronit Microtechnologies B.V., Netherlands. A Micronit Fluidic Connect Pro chip holder houses the microchip to ensure proper confinement and prevent fluid leaks during flow tests. Table 1 shows the dimensions of the microchannels in the chip while Figure 1 shows the chip holder and a detailed description of the microchip.

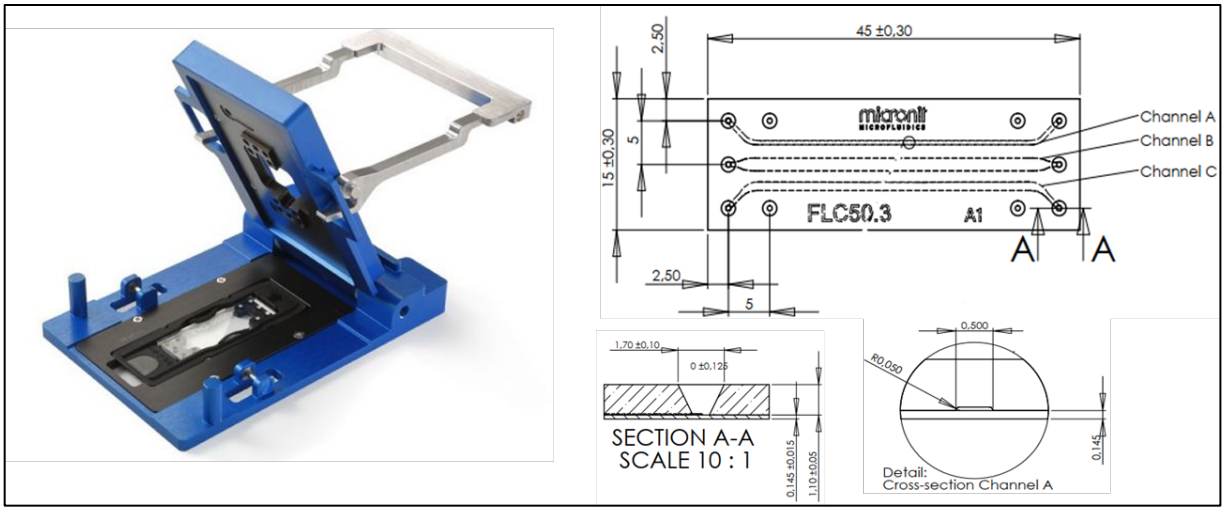

Figure 1: Pictorial description of the Fluidic Connect Pro chip holder (left) and the Microchip (right) (www.micronit.com)

Table 1: Dimensions of Microchannels.

Channel	Width (mm)	Length (mm)	Depth (mm)	Volume (µl)
A	0.5	42	0.05	1
B	1.5	40	0.05	2.8
C	1	42	0.05	1.9

2.2 Test Fluids

Two (ILs), 1-butyl-3-methyl-imidazolium bromide ([bmim][Br]) and 1-hexylpyridinium bromide ([hPy][Br]), were used to conduct the flow tests. The results obtained from the ILs were compared against those from deionized (DI) water). In addition, aqueous solutions of [bmim][Br] and [hPy][Br] were tested at three different concentrations of the ILs. The properties of the ILs, determined by Atashnezhad et al., (2023), are presented in Table 2 below.

Table 2: Properties of test fluids (Atashnezhad et al., 2023).

Fluids	Viscosity @ SR = 25-100 1/s & P = ~ 101.5 psi (cP)	Density (g/cc)	Thermal Stability (ºC)
[bmim][Br]	199-364	0.94	280
[hPy][Br]	697-715	1.105	380
DI Water	1	1.000	---

The viscosities of the aqueous test fluids were determined using a RheoSense microVISC viscometer. The viscometer uses an array of pressure sensors to measure the force required to pump fluids through a rectangular microfluidic channel which is indicative of the fluid's resistance to flow. Analytical solutions, such as the Hagen-Poiseuille equation, are then applied to estimate the shear stress and viscosity from the measured pressure drop. The densities of the aqueous samples were measured using a densitometer (Mettler Toledo DA-100M). The densitometer uses

the vibration frequency of a liquid-filled U-tube to determine the density of the liquid. Table 3 shows the viscosity and density of aqueous solutions of the ILs at 18 ^{o}C.

Table 3: Properties of test fluids continued.

	Viscosity @ 18 ^{o}C (cP)	**Density (g/cc)**
5% [bmim][Br]	1.402	1.0070
10% [bmim][Br]	1.528	1.0140
25% [bmim][Br]	2.007	1.0437
5% [hPy][Br]	1.258	1.0100
10% [hPy][Br]	1.340	1.0200
25% [hPy][Br]	1.791	1.0507

2.3 Experimental Facility

The microfluidic facility used to evaluate the reversibility of the ILs consists of several key components: i) constant pressure and constant rate syringe pumps for injecting and withdrawing the liquids into and from the chip; ii) a microchip and chip holders to simulate flow through fractures in EGS; iii) control valves; iv) differential pressure sensors to measure the pressure difference between the inlet and outlet of the microchip; v) a data acquisition device (DAQ) for real-time data gathering and performance analysis; vi) a workstation to monitor flow through the microchannels; vii) various fittings and PEEK tubings to facilitate fluid flow across the microchip. Figure 2 illustrates the process flow diagram of the experimental setup. For multichannel experiments, the Tee connectors at the inlet and outlet of the microchip are replaced by a union cross. The microchip features three idealized microfractures of varying widths but roughly the same length and depth.

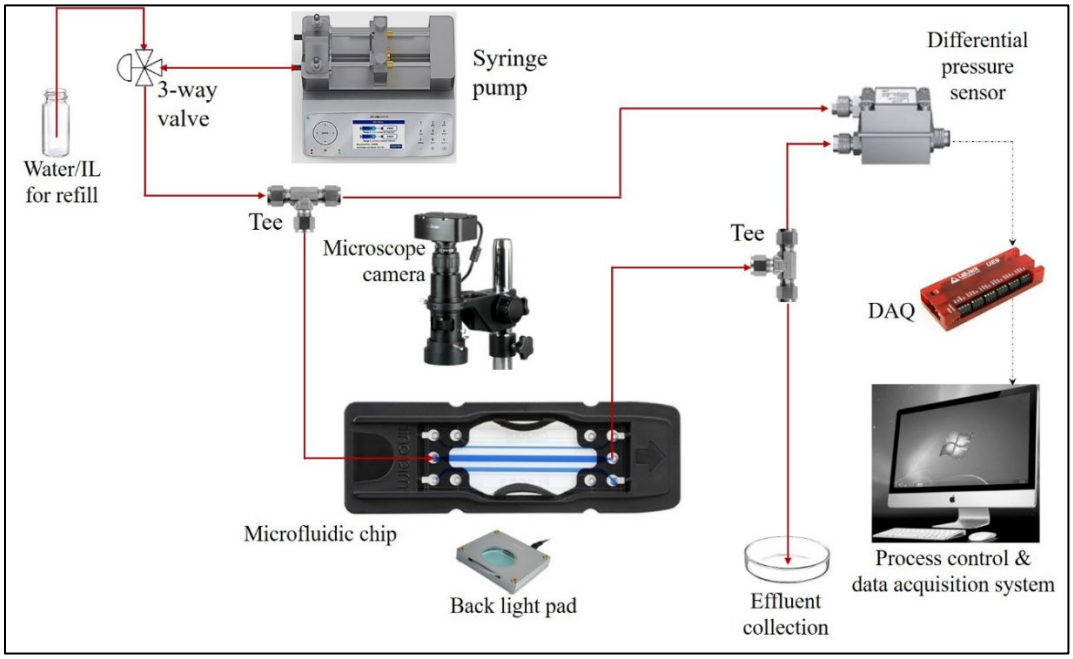

Figure 2: Process flow diagram for the experimental setup to conduct flow tests across the microchannel(s)

2.4 Pressure Drop across the Microfluidic Channels

A TDK minicell pressure sensor was used to measure the differential pressure across the microchannel(s). The pressure sensor records the voltage difference between the inlet and the outlet of a microchannel based on the piezoelectric effect. The measured voltage is transmitted through a LabJack UE9pro data acquisition device to a computer monitor. To convert the recorded voltage values to differential pressure (ΔP), the pressure sensor was calibrated to obtain a relation between voltage (V) and pressure drop (psi). The calibration was performed using a constant pressure injection pump (make: Teledyne ISCO; model: 260 D), yielding a linear relationship between the differential pressure and the voltage ($\Delta P = 35.711V - 17.162$, $R^2 = 0.9999$), as shown in Figure 3. This linear model was used to estimate ΔP from the voltage values recorded during the different flow experiments. By maintaining a constant flow rate through the microchannels, we recorded voltage values and applied the linear model to estimate ΔP which provided insights into the behavior of ILs in EGS.

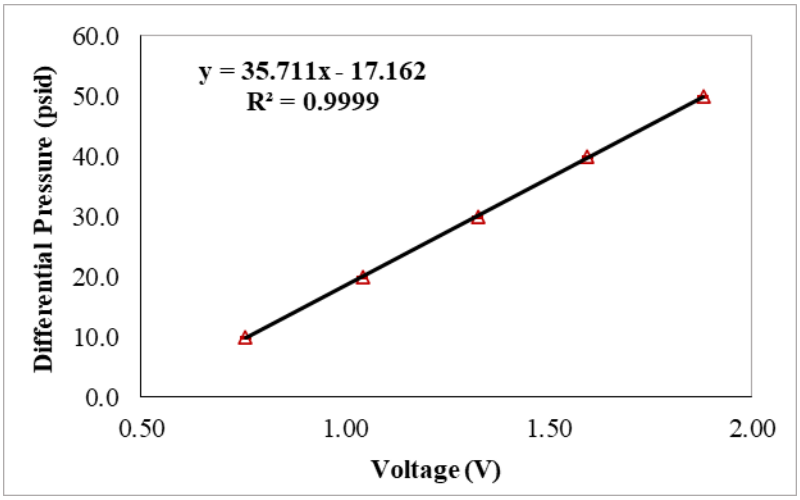

Figure 3: Calibration curve for the differential pressure sensor.

2.5 Procedures for Determining the Pressure Drop across the Microchannel(s)

2.5.1 Low Temperature Experiments

A Havard PHD Ultra syringe pump was used to conduct low-temperature experiments. Test fluids are withdrawn from the fluid reservoir into the syringe pump. They are then injected into the microchannel at a constant flow rate at room temperature (18 ^{o}C). The ΔPs across single microchannels are estimated using stabilized voltage readings i.e., when steady state flow exists in the microchannels. The flow rate is initially increased in steps until a predetermined rate is attained with the stabilized voltage values recorded at each flow rate. Next, the flow rate is reduced from the maximum to the minimum rate in the previous cycle while maintaining the same flow rate intervals. Finally, the flow rate is increased again from the lowest to the highest rate using the same step intervals in the first two cycles. This sequence is repeated for each test fluid, and the average of all three voltage values is used to estimate the pressure drop across the microchannel(s).

To minimize contamination of the test liquids, the microchannels and the pump's syringe are thoroughly cleaned with DI water and isopropyl alcohol (IPA) between experiments. This entire procedure is repeated for each test fluid and for both single- and two-channels.

2.5.2 High Temperature Experiments

For high-temperature experiments, a Chemyx Fusion 6000X syringe pump was used. Chemyx Fusion 6000X pump was used to pre-heat, regulate, and maintain the temperature of fluids in its syringe. The test fluids were preheated in a water bath to the desired temperature before withdrawing the liquids into the pump's syringe. The pump is then used to preheat the fluid again before injecting it into the microchannel. A thermal insulation tape was used to wrap the components of the setup, including the syringe, tubings, and fittings, to minimize heat losses. The procedures utilized to determine the pressure drop at the room temperature experiments were also adopted for the high-temperature experiments.

3. Results And Discussion

3.1 Aqueous Solutions

ILs may be diluted by water when utilized as geothermal working fluids, especially in hot wet rocks (HWR). It is therefore necessary to understand the flow behavior of aqueous solutions of the ILs utilized in this study. Flow behavior of 5%, 10%, and 25% solutions of [bmim][Br] and [hPy][Br] in the microchannels were examined in this work. The pressure drop vs. flowrate curves for these solutions are presented in the following sections.

3.1.1 Results for [bmim][Br]

The flow of fluid from one point to another in a system generally leads to a reduction in pressure due to three main factors: kinetic losses, potential losses, and frictional losses. The microfluidic setup consists of horizontally positioned and uniformly sized microchannels, thus eliminating potential and kinetic losses respectively. Frictional loss is a measure of a fluid's resistance to flow and is dependent on the fluid and system properties. Analytical solutions describing flow through microfluidic channels have shown that the pressure drop across microfluidic channels is dependent on the flowrate, fluid properties, and dimensions of the channel(s) (Estarki et al., 2023; Joseph et al., 2013). The viscosity of the fluid is the main fluid property that affects pressure drop, it describes the internal resistance of the fluid to flow. Thus, the more viscous the IL/aqueous solution, the higher its internal resistance and the consequent differential pressure across the channel/multichannel. Figure 4 shows the variation of pressure drop with flowrate for aqueous solutions of [bmim][Br] in single- and two-channels. It can be observed that the recorded ΔP increased with flowrate in all the cases considered. In addition, for a fixed flow rate, the pressure drop increased with increasing concentration of the [bmim][Br]. The increased pressure drop can be attributed to an increase in viscosity as the concentration of the IL increased from 5% to 25%. Readers are referred to Table 3 for the viscosities of the test fluids. Similarly, the differential pressure reduced with increase in the width of the channels because shear rate and flow resistance decreases as the width of the channels increases. This behavior was also noted in the two-channel experiments where the pressure drop derived from flowing through the single channel was always higher than the pressure drop recorded when a second channel was combined. The error bars on each data point in the plots represent the standard deviations of the mean ΔP value from three ΔP data points recorded in distinct experiments.

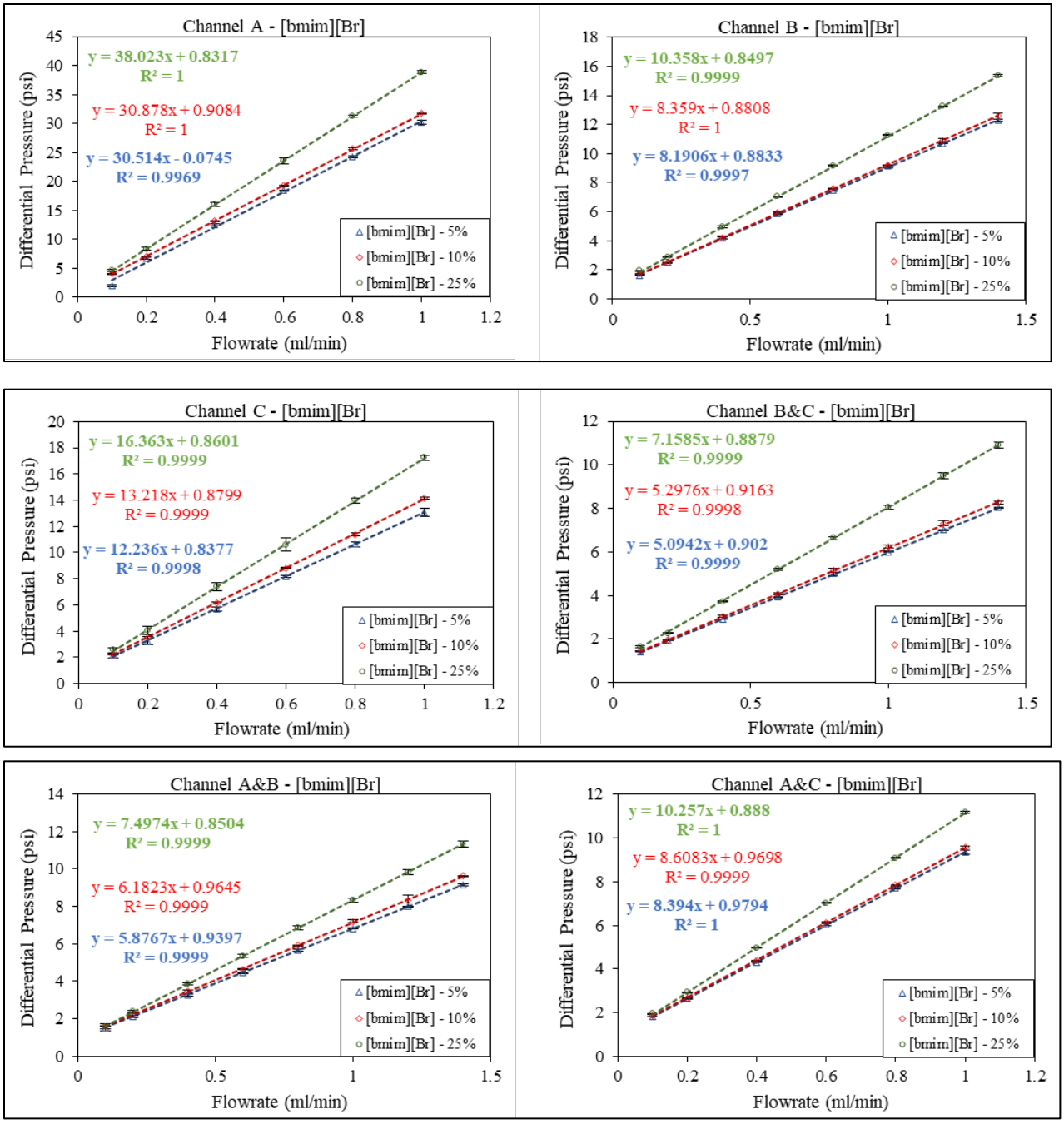

Figure 4: Variation of pressure drop (ΔP) with flow rate of [bmim][Br] in the microchannels

3.1.2 Results for [hPy][Br]

Similar trends were observed in the [hPy][Br] solutions as with the aqueous [bmim][Br] solutions. The pressure drop increased with both flowrate and concentration of the ILs, while it decreased with increasing channel width. It is important to note that the viscosity of 5% and 10% samples are closer compared to that of 10% and 25% concentrations which could explain the comparable ΔP-Q trends for 5% and 10% in all the cases.

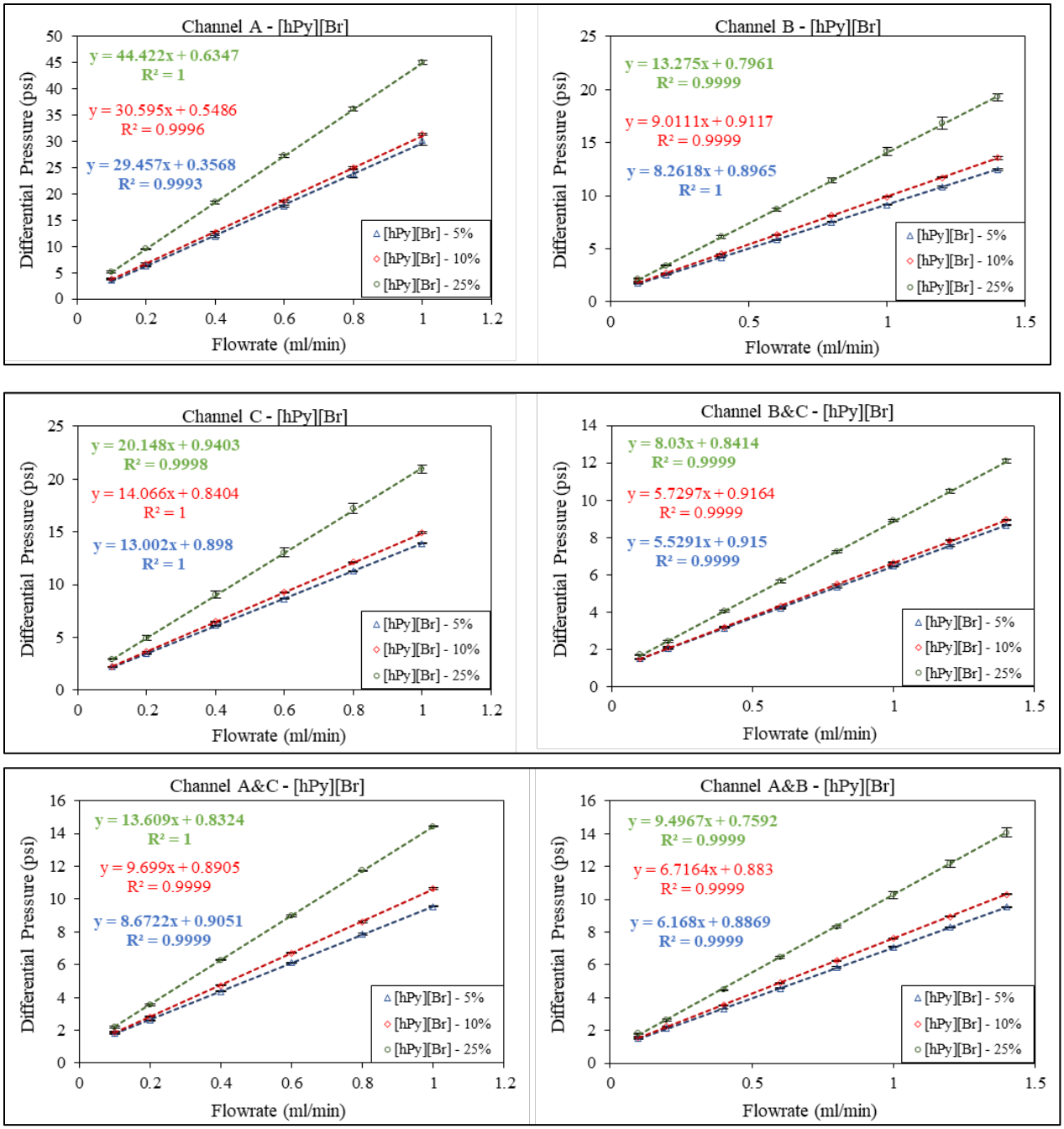

Figure 5: Variation of pressure drop (ΔP) with flow rate of [hPy][Br] in the microchannels

3.2 Results for [bmim][Br] and DI Water at High Temperature

Figures 6 and 7 show the effect of increasing the temperature of the DI water and [bmim][Br] on the pressure drop across a microchannel. As stated in previous sections, the pressure drop across each channel results from the frictional losses in the system which are mainly dependent on the viscosity of the flowing liquid and the internal conditions of the channel such as roughness, and channel dimensions. Temperature dependence of viscosity varies from fluid to fluid. The viscosity of [bmim][Br] reduces significantly when the temperature is increased. Thus, the measured pressure

drop across the channel at a constant rate reduces as the temperature of the IL increases. DI water, on the other hand, does not experience much viscosity reduction with increasing temperatures. For example, Korson et al., in 1969 estimated the viscosity of DI water at a temperature range of 0-100 ºC. The viscosities of DI water at 18 ºC, 50 ºC, and 80 ºC are approximately 1 cP, 0.55 cP, and 0.35 cP, respectively. As shown in Figure 6, the pressure drop across the channels did not change much when the temperature of DI water was increased from 18ºC to 50ºC and 80ºC.

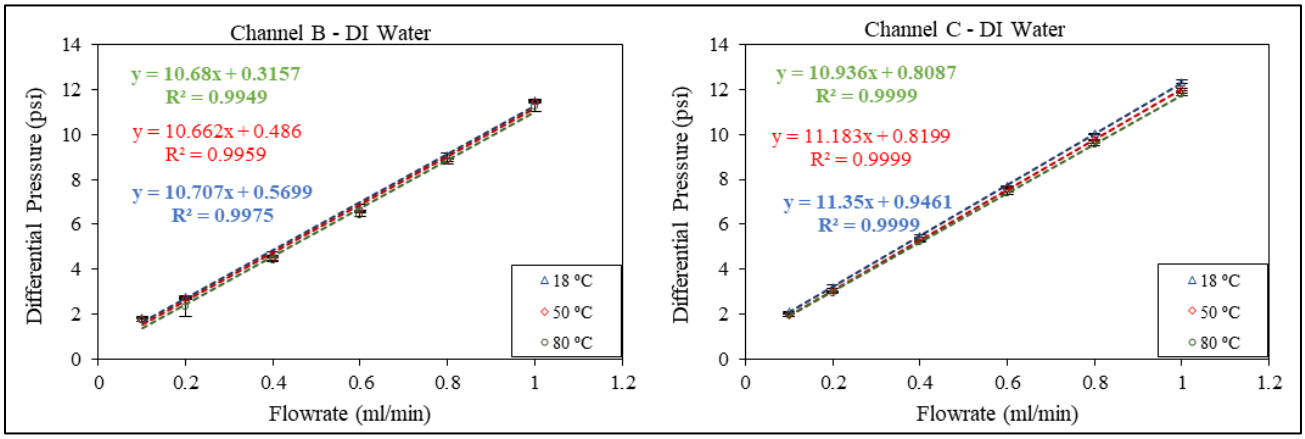

Figure 6: Variation of pressure drop (ΔP) with flow rate of DI water at 18 °C, 50 °C, and 80 °C in channel B and channel C

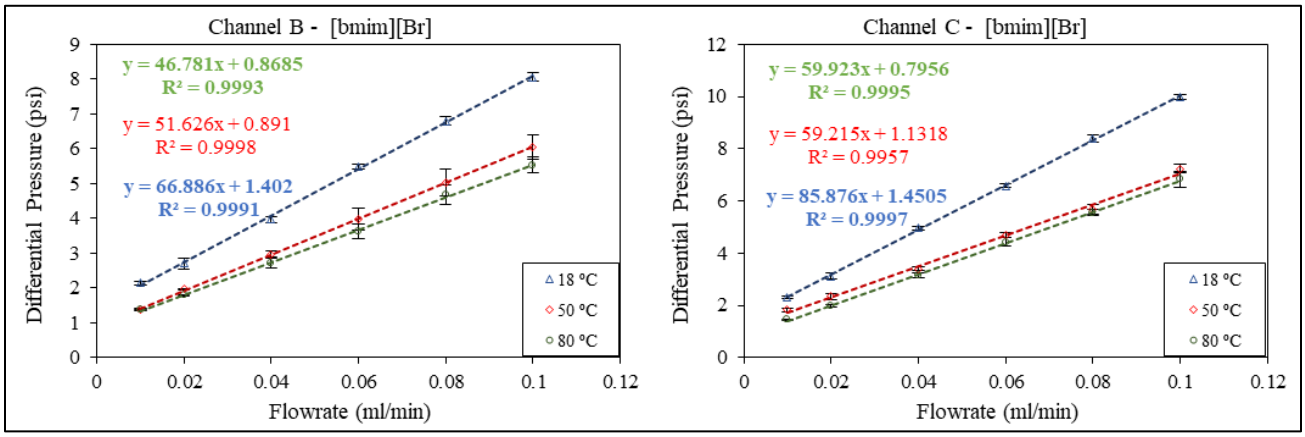

Figure 7: Variation of pressure drop (ΔP) with flow rate of [bmim][Br] at 18 °C, 50 °C, and 80 °C in channel B and channel C

Figure 6 and 7 demonstrates that [bmim][Br] exhibits enhanced hydrodynamic properties with increasing temperature compared to DI water at the microscale. This is further illustrated in Table 4 which shows the percentage reduction in pressure drop for both DI water and [bmim][Br], when a constant flow rate of 0.1 ml/min was maintained for both liquids.

Table 4: Recorded ΔP values and percent change of ΔP with temperature increase from 18°C to 80°C for DI water and [bmim][Br] in Channel B and Channel C.

Test fluid	Channel B						Channel C					
	DI Water			[bmim][Br]			DI Water			[bmim][Br]		
Temperature (°C)	18	50	80	18	50	80	18	50	80	20	50	80
ΔP (psi)	1.84	1.76	1.75	8.06	6.05	5.53	2.11	1.94	1.94	9.99	7.24	6.82
Percent reduction in ΔP	--	3.89	4.54	--	24.95	31.38	--	7.9	7.9	--	27.52	31.69

The frictional pressure loss reduction ratio, derived by comparing the percent reduction in ΔP of [bmim][Br] with that of DI water, is shown in Table 5.

Table 5: Frictional pressure loss reduction ratio of [bmim][Br] with respect to DI water.

Channel	Channel B		Channel C	
Temperature (°C)	50	80	50	80
Frictional pressure loss reduction ratio	6.4	6.9	3.5	4

Tables 4 and 5 show that the percent reduction in differential pressure with increasing temperature for DI water is much lower than the reduction experienced with [bmim][Br]. [bmim][Br] outperforms DI water in terms of the reduction in the frictional pressure loss in microchannels with increasing temperature. In channel B, [bmim][Br] exhibited a frictional pressure loss reduction seven times greater than that of DI water, while in channel C, it showed a four-fold reduction compared to DI water.

3.3 EGS Implications

As stated earlier, flow channeling can lead to thermal short-circuiting which can negatively impact the overall heat recovery efficiency of an EGS project. Unlike water, ILs have temperature-dependent viscosities, which can prevent thermal short-circuiting. As the viscosity of ILs increases in highly conductive, low-temperature flow paths, flow resistance increases, redirecting the ILs to lower conductivity, higher temperature paths. This redistribution into smaller, hotter fractures enhances the recovery efficiency of an EGS and can extend the project's lifespan. We can infer from the results that the use of [bmim][Br] (and similar ILs) as geothermal working fluids leads to greater frictional pressure loss which could cause more fluid flow in low-conductivity fractures. It is important to note that these experiments were conducted at a maximum temperature of 80°C due to the limitations of our experimental facility. In reality, higher temperatures exceeding 180°C have been recorded in EGS (Lu, 2018). Therefore, the frictional pressure loss ratio is expected to increase under actual EGS conditions, leading to improved flow hydraulics. However, drawing definitive conclusions from these findings requires further study to verify the flow behavior of ILs in fracture networks at the elevated temperatures typical of geothermal reservoirs.

4.0 Conclusions

The flow behaviors of [bmim][Br] and [hPy][Br] within idealized microfractures were evaluated using a microfluidic setup, and their potential as geothermal working fluids was discussed. The main findings from this study are:

- The ILs demonstrated pressure drops across single and multichannel proportional to the flowrate, viscosity of the ILs, and the dimensions of the single- and two-channels. [bmim][Br] showed a significant reduction in the frictional loss compared to DI water. The frictional pressure loss reduction of [bmim][Br] at 80^{o}C was about seven times that of DI water in channel B and four times greater than DI water in channel C.
- In EGS reservoir conditions, we expect a much higher viscosity increase ratio for the ionic liquids when temperature declines which can potentially eliminate short circuits.
- The use of ILs presents a dynamic solution to fracture tuning, enhancing the overall heat recovery and performance of EGS.

5.0 Acknowledgement

The research is based on work funded by the Department of Energy Office of Energy Efficiency and Renewable Energy (EERE) under the Geothermal Program Office Award Number DE-EE0009788.

We also thank our research collaborators Dr Al Dushaishi M., and Dr Atashnezhad A., for their work on the synthesis and characterization of the ILs.

References

Al Balushi, F., Zhang, Q., & Dahi Taleghani, A. (2023). Improving enhanced geothermal systems performance using adaptive fracture conductivity. *Applied Thermal Engineering*, *233*, 121206. https://doi.org/10.1016/j.applthermaleng.2023.121206.

André, L., Rabemanana, V., & Vuataz, F.-D. (2006). Influence of water-rock interactions on fracture permeability of the deep reservoir at Soultz-sous-Forêts, France. *Geothermics*, *35*(5), 507–531. https://doi.org/10.1016/j.geothermics.2006.09.006.

Asai, P., Panja, P., McLennan, J., & Deo, M. (2019). Effect of different flow schemes on heat recovery from Enhanced Geothermal Systems (EGS). *Energy*, *175*, 667–676. https://doi.org/10.1016/j.energy.2019.03.124.

Atashnezhad, A., Akhtarmanesh, S., Kjeldal, V. N., & Dushaishi, M. F. A. (2023). *Advancing Enhanced Geothermal Reservoirs with Ionic Liquids as Potential Geothermal Fluid*.

Bertani, R. (2016). Geothermal power generation in the world 2010–2014 update report. *Geothermics*, *60*, 31–43. https://doi.org/10.1016/j.geothermics.2015.11.003.

Brown, D. W. (2000). *A hot dry rock geothermal energy concept utilizing supercritical CO2 instead of water, PROCEEDINGS, Twenty-Fifth Workshop on Geothermal Reservoir Engineering Stanford University*. Stanford, California, January.

Emujakporue, G. O. (2017). Subsurface temperature distribution from heat flow conduction equation in part of chad sedimentary basin, Nigeria. *Egyptian Journal of Petroleum*, *26*(2), 519–524. https://doi.org/10.1016/j.ejpe.2016.07.003.

Estarki, H. E., Tareie, Z. S., & Latifi, H. (2023). Pressure drop measurement in microfluidics channel by the Fabry-Perot diaphragm-based flow sensor. *Flow Measurement and Instrumentation*, *91*, 102355.

Fan, H., Zhang, L., Wang, R., Song, H., Xie, H., Du, L., & Sun, P. (2020). Investigation on geothermal water reservoir development and utilization with variable temperature regulation: A case study of China. *Applied Energy*, *275*, 115370. https://doi.org/10.1016/j.apenergy.2020.115370.

Fu, P., Hao, Y., Walsh, S. D. C., & Carrigan, C. R. (2016). Thermal Drawdown-Induced Flow Channeling in Fractured Geothermal Reservoirs. *Rock Mechanics and Rock Engineering*, *49*(3), 1001–1024. https://doi.org/10.1007/s00603-015-0776-0.

Gischig, V. S., & Preisig, G. (2015). Hydro-fracturing versus Hydro-shearing: a critical assessment of two distinct reservoir stimulation mechanisms.

Guo, B., Fu, P., Hao, Y., Peters, C. A., & Carrigan, C. R. (2016). Thermal drawdown-induced flow channeling in a single fracture in EGS. *Geothermics*, *61*, 46–62. https://doi.org/10.1016/j.geothermics.2016.01.004.

Guo, T., Gong, F., Wang, X., Lin, Q., Qu, Z., & Zhang, W. (2019). Performance of enhanced geothermal system (EGS) in fractured geothermal reservoirs with CO2 as working fluid. *Applied Thermal Engineering*, *152*, 215–230. https://doi.org/10.1016/j.applthermaleng.2019.02.024.

Hu, X., Song, X., Wu, K., Shi, Y., & Li, G. (2021). Effect of proppant treatment on heat extraction performance in enhanced geothermal system. *Journal of Petroleum Science and Engineering*, *207*, 109094. https://doi.org/10.1016/j.petrol.2021.109094.

Joseph, J., Siva Kumar Gunda, N., & Mitra, S. K. (2013). On-chip porous media: Porosity and permeability measurements. *Chemical Engineering Science*, *99*, 274–283. https://doi.org/10.1016/j.ces.2013.05.065.

Korson, L., Drost-Hansen, W., & Millero, F. J. (1969). Viscosity of water at various temperatures. *The Journal of Physical Chemistry*, *73*(1), 34–39. https://doi.org/10.1021/j100721a006

Lei, H. (2022). Performance Comparison of H_2O and CO_2 as the Working Fluid in Coupled Wellbore/Reservoir Systems for Geothermal Heat Extraction. *Frontiers in Earth Science*, *10*, 819778.

Li, S., Wang, S., & Tang, H. (2022). Stimulation mechanism and design of enhanced geothermal systems: A comprehensive review. *Renewable and Sustainable Energy Reviews*, *155*, 111914.

Li, T., Shiozawa, S., & McClure, M. W. (2016). Thermal breakthrough calculations to optimize design of a multiple-stage Enhanced Geothermal System. *Geothermics*, *64*, 455–465. https://doi.org/10.1016/j.geothermics.2016.06.015.

Lu, S.-M. (2018). A global review of enhanced geothermal system (EGS). *Renewable and Sustainable Energy Reviews*, *81*, 2902–2921. https://doi.org/10.1016/j.rser.2017.06.097.

Momoh, I., Lee, H., Atashnezhad, A., & Al Dushaishi, M. (2023). *Fracture Conductivity Tuning in Granite under Triaxial Loading using Ionic Liquids: Implications for Enhanced Geothermal Systems*.

Olasolo, P., Juárez, M. C., Morales, M. P., D´Amico, S., & Liarte, I. A. (2016). Enhanced geothermal systems (EGS): A review. *Renewable and Sustainable Energy Reviews*, *56*, 133–144. https://doi.org/10.1016/j.rser.2015.11.031.

Smith, M. C., Aamodt, R. L., Potter, R. M., & Brown, D. W. (1975). *Man-made geothermal reservoirs*. Los Alamos Scientific Lab., N. Mex.(USA). https://www.osti.gov/servlets/purl/5132450.

Sun, F., Yao, Y., Li, G., & Li, X. (2018). Performance of geothermal energy extraction in a horizontal well by using CO2 as the working fluid. *Energy Conversion and Management*, *171*, 1529–1539. https://doi.org/10.1016/j.enconman.2018.06.092.

Zhang, Q., & Dahi Taleghani, A. (2023). Autonomous fracture flow tunning to enhance efficiency of fractured geothermal systems. *Energy*, *281*, 128163. https://doi.org/10.1016/j.energy.2023.128163.